Single-molecule live-cell imaging visualizes parallel pathways of prokaryotic nucleotide excision repair

Harshad Ghodke[1,2*], Han Ngoc Ho[1,2], Antoine M van Oijen[1,2]

[1]Molecular Horizons and School of Chemistry and Molecular Bioscience, University of Wollongong, Wollongong, New South Wales, 2522, Australia

[2] Illawarra Health and Medical Research Institute, Wollongong, New South Wales, 2522, Australia

Correspondence: Harshad Ghodke (harshad@uow.edu.au)

Abstract:

In the model organism *Escherichia coli,* helix distorting lesions are recognized by the UvrAB damage surveillance complex in the global genomic nucleotide excision repair pathway (GGR). Alternately, during transcription-coupled repair (TCR), UvrA is recruited to Mfd at sites of RNA polymerases stalled or paused by lesions. Ultimately, damage recognition is mediated by UvrA, culminating in the loading of the damage verification enzyme UvrB. We set out to characterize the differences in the kinetics of interactions of UvrA with Mfd and UvrB. We followed functional, fluorescently tagged UvrA molecules in live cells and measured their residence times in TCR-deficient or wild-type cells. We demonstrate that the lifetimes of UvrA in Mfd-dependent or Mfd-independent interactions in the absence of exogenous DNA damage are comparable in live cells, and are governed by UvrB. Upon UV irradiation, we found that the lifetimes of UvrA strongly depended on, and matched those of Mfd. Here, we illustrate a non-perturbative, imaging-based approach to quantify the kinetic signatures of damage recognition enzymes participating in multiple pathways in cells.

Introduction

Across the various domains of life, the recognition and repair of bulky, helix-distorting lesions in chromosomal DNA is coordinated by nucleotide excision repair (NER) factors. Damage detection occurs in two stages: a dedicated set of damage surveillance enzymes (reviewed in ref.[1, 2, 3]) (namely the prokaryotic UvrA, and the eukaryotic UV-DDB, XPC, XPA and homologs) constantly survey genomic DNA for lesions. At sites of putative DNA damage, these enzymes load specific factors (UvrB in prokaryotes, TFIIH and homologs in eukaryotes) that unwind the DNA and verify the location of the damage with nucleotide resolution (Fig. 1a) (reviewed in ref.[2, 3]). Subsequently, specialized endonucleases (prokaryotic UvrC and homologs, and the eukaryotic XPF-ERCC1/XPG and homologs) are recruited to the site of the DNA, resulting in cleavage of the single-stranded DNA (ssDNA) patch containing the lesion (reviewed in ref.[2, 3]).

In several studied organisms (barring certain archaea[4, 5]), removal of DNA damage also occurs via the triggering of strand-specific DNA repair following the stalling of RNA polymerase (RNAP) at sites of lesions (reviewed in ref.[6]). In this case, a ternary elongation complex (TEC) of RNAP that is unable to catalyse nascent RNA synthesis manifests as an ultra-stable protein-DNA roadblock. Transcription-repair coupling factors such as the prokaryotic Mfd, and the eukaryotic homologs Rad26/CSB are dedicated factors that recognize these TECs and remodel them[7, 8, 9, 10, 11]. In prokaryotes, Mfd is recruited to the site of a failed TEC, and in turn it recruits the $UvrA_2B$ complex via interactions between its UvrB-homology module (BHM) and UvrA. (Fig. 1) [9, 11, 12, 13]. Similarly, in eukaryotes, CSB is recruited to the site of a stalled RNAPII complex, and recruits the TFIIH complex[14].

DNA repair triggered by stalling of TECs is termed transcription-coupled repair (TCR), in contrast to the direct detection of lesions by the UvrAB damage sensor (global genomic repair, or GGR). Studies investigating the rate of repair during TCR *vs*. GGR, have reported an enhancement in the rate of removal of UV-induced lesions from the template strand in transcribed DNA compared to non-transcribed DNA[15, 16, 17, 18, 19, 20]. This observation has sparked several studies targeted at understanding the mechanistic basis of rate enhancement[13, 21, 22]. A recent single-molecule *in vitro* study reported that the time to incision in TCR is approximately three-fold faster than in GGR under certain conditions [13].

A diverse set of intermediates is readily formed *in vitro* - ranging from a translocating RNAP-Mfd complex, arrested RNAP-Mfd-$UvrA_2$ and the complete Mfd-$UvrA_2$-UvrB handoff complex in the presence of both UvrA and UvrB[12, 13]. To understand which of these intermediates are formed inside cells, we have recently visualized Mfd in cells and quantified its lifetime in the TCR reaction[12]. A recent

56 study failed to detect an influence of Mfd on the behaviour of fluorescently tagged UvrA in living
57 cells[23]. Therefore, *in vitro* studies notwithstanding, how TCR is orchestrated by UvrA in cells remains
58 unclear.

59 In this work, we revisited this question in the context of live cells and applied high-resolution single-
60 molecule imaging methods that permit accurate measurements of DNA binding lifetimes over a broad
61 timescale ranging from a few hundred milliseconds to several minutes[12, 24]. We asked the question:
62 what is the lifetime of interactions of UvrA with Mfd and UvrB? To answer this question, we visualized
63 fluorescently tagged UvrA in cells and measured the lifetimes of the interactions with DNA in wild-
64 type and TCR-deficient cells. We find that UvrA is long lived on DNA in the absence of UvrB and Mfd,
65 and that its dissociation is promoted by UvrB in cells. The cellular concentration of UvrA relative to
66 UvrB strongly influences its binding lifetime in interactions with DNA-bound Mfd. The binding lifetimes
67 of Mfd-UvrA interactions are only detected under conditions of limiting UvrB in the absence of
68 exogenous DNA damage, suggesting a role for UvrB in resolving Mfd-UvrA intermediates. Exposure to
69 ultraviolet light (UV) leads to an increase in the binding lifetime of UvrA in TCR-deficient cells. In
70 contrast, in TCR-proficient cells, the DNA-bound lifetimes of UvrA and Mfd are identical, and drop
71 upon UV exposure suggesting the formation of an Mfd-UvrA intermediate in TCR. Together, these
72 studies characterize the interaction of UvrA with Mfd in live cells. Here, we establish a comprehensive
73 framework for characterizing the binding kinetics of DNA repair proteins participating in multiple
74 parallel pathways *in vivo* using non-perturbative, single-molecule imaging approaches.

75 **RESULTS**

76 The nucleotide excision repair reaction can be considered to occur in five discrete stages: damage
77 recognition, damage verification, incision, repair synthesis and ligation (reviewed in ref[2]). UvrA
78 mediates damage recognition by itself and by interacting with Mfd[1]. It does so by surveying the
79 genome constantly for the presence of DNA damage or for Mfd-bound TECs. Following DNA binding
80 at a putative damage site, damage verification is then orchestrated by the damage verification enzyme
81 UvrB[25]. Surprisingly, UvrA by itself has relatively poor specificity for binding to DNA damage over
82 undamaged DNA[26]. Here, we set out to characterize the kinetic states that describe damage
83 surveillance and loading of UvrB in live cells.

84 **Imaging of UvrA-YPet in the absence of exogenous DNA damage**

85 To visualize the binding of UvrA to DNA in cells, we replaced the *uvrA* gene with a C-terminal fusion of
86 *uvrA* to the gene for the yellow fluorescent protein (YPet[27]) in MG1655 cells using λ Red recombination
87 (Fig. 2a)[12, 28]. This strategy enabled observation of fluorescent UvrA-YPet expressed from the native,

88 SOS-inducible *uvrA* promoter (Supplementary Movie 1). We first performed UV-survival assays to
89 assess the ability of UvrA-YPet to execute nucleotide excision repair (NER). Compared to wild-type
90 cells, *uvrA-YPet* cells exhibited somewhat poorer survival upon exposure to UV (Supplementary Fig.
91 1a). Considering that C-terminal fusions of UvrA are fully functional in NER[23, 29], this modestly lower
92 survival of *uvrA-YPet* cells may be attributable to a lower efficiency of protein translation.

93 Therefore, we set out to measure the copy numbers of UvrA-YPet in *uvrA-YPet* cells grown in EZ-rich
94 defined media supplemented with glucose at 30 °C. Exponentially growing cells were deposited on a
95 modified glass coverslip at the bottom of a flow cell and visualized by illumination with 514-nm laser
96 light under continuous flow of growth medium (Fig. 2b). Images of *uvrA-YPet* cells revealed DNA-
97 bound UvrA-YPet molecules that manifested as static foci and diffusive molecules contributing to
98 cellular background fluorescence (Fig. 2c). These observations are consistent with its role as a damage
99 surveillance protein.

100 Exposure to laser light led to rapid loss of YPet signal due to photodarkening and photobleaching of
101 the chromophore (Supplementary Movie 1). We used this loss of signal to measure copy numbers of
102 UvrA-YPet in cells. Dividing the background-corrected cellular fluorescence intensity by the intensity
103 of a single YPet molecule revealed a copy number of 16 ± 4 copies of UvrA-YPet per cell
104 (Supplementary Fig. 1b-d). Copy numbers of UvrA are strongly influenced by the carbon source
105 present in the growth medium, ranging from 9 - 43 copies (minimal media) to 129 copies (rich media)
106 per cell [30]. These estimates exceed the copy numbers of UvrA-YPet detected in the *uvrA-YPet* strain
107 grown in rich medium. The lower copy numbers of UvrA-YPet are consistent with the minor
108 deficiencies in survival observed after UV exposure (Supplementary Fig. 1a).

109 To confirm the hypothesis that the deficiencies in UV survival observed for the *uvrA-YPet* strain are
110 attributable to lower copy numbers as opposed to a catalytically deficient protein, we created a low
111 copy plasmid (pSC101 origin of replication, 3-4 copies/cell[31]) expressing the C-terminal YPet fusion of
112 UvrA under its native promoter (pUvrA-YPet). We then transformed Δ*uvrA* cells with pUvrA-YPet.
113 These cells express UvrA-YPet to the extent of 120 ± 28 copies per cell (Supplementary Fig. 1b-d). UV
114 survival assays (Supplementary Fig. 1e) revealed that UvrA-YPet expressed from the plasmid is able to
115 fully complement the Δ*uvrA* phenotype. Therefore, we conclude that the copy numbers of UvrA-YPet
116 expressed from the endogenous *uvrA* promoter represent lower copy numbers compared to untagged
117 UvrA expressed in wild-type cells, likely reflecting a poorer efficiency of translation of the *uvrA-YPet*
118 gene.

119 **Interval imaging strategy to measure DNA binding kinetics**

120 Continuous imaging of UvrA-YPet could not be used to measure DNA binding lifetimes, since the
121 apparent lifetime of a focus represents UvrA-YPet molecules dissociating from the site or bound UvrA-
122 YPet molecules that are photobleached during the imaging. Consequently, measurement of
123 interactions that last longer than the photobleaching lifetime is impossible. Instead we imaged UvrA-
124 YPet using a strategy of performing time-lapse imaging with dark periods of varying intervals (for
125 brevity, we term this mode of imaging 'interval imaging')[12, 24, 32, 33] (Fig. 2d) that elegantly deconvolutes
126 the lifetime of the interaction of UvrA-YPet with DNA and the lifetime of the fluorescent probe. Briefly,
127 the introduction of a dark interval (τ_d) between consecutive frames of duration (τ_{int}) extends the
128 observation time window. Here the time between consecutive frames is denoted as time-lapse time
129 (τ_{tl}). By acquiring the same number of frames in each video collected with a different dark interval,
130 the photobleaching rate (k_b) is maintained constant (see Table 1 and Methods) while the observation
131 window is extended arbitrarily. From these videos, cumulative residence time distributions of DNA-
132 bound UvrA-YPet are constructed. Since these distributions reflect a mixture of two populations (UvrA
133 molecules that dissociate and YPet molecules that photobleached), fitting them to an exponential
134 function yields an effective off rate (k_{eff})[32]. The product ($k_{eff}\tau_{tl}$) is a linear function of true off rate ($k_{off}\tau_{tl}$)
135 and the normalized photobleaching rate ($k_b\tau_{int}$)[32]. For purposes of illustration, the data can be
136 represented as $k_{eff}\tau_{tl}$ *vs.* τ_{tl} plots where the slope reveals the off rate k_{off} and the Y-intercept reveals k_b.
137 This interval imaging strategy enables accurate quantification of binding lifetimes over three orders of
138 magnitude from 0.1 s to several minutes[12, 32, 34].

139 **UvrA is long-lived on DNA in the absence of UvrB and Mfd**

140 First, we interrogated UvrA binding kinetics in the absence of its two major interacting partners UvrB
141 and Mfd in growing cells. To that end, we transformed cells lacking UvrA, UvrB and Mfd (Δ*uvrA* Δ*uvrB*
142 Δ*mfd* cells) with pUvrA-YPet. In these cells, we expected that interactions of UvrA-YPet with
143 chromosomal DNA would reflect two of its key activities: binding to non-damaged DNA and binding
144 to endogenous DNA damage produced as a by-product of cellular metabolism (Fig. 3a). Indeed,
145 measurements of UvrA-YPet kinetics of dissociation in these cells revealed two lifetimes that are an
146 order of magnitude apart - a fast lifetime ($\tau_{UvrA|\Delta uvrA\ \Delta uvrB\ \Delta mfd,\ fast}$) of 1.6 ± 0.1 s (72 ± 2 %) and a slow
147 lifetime ($\tau_{UvrA|\Delta uvrA\ \Delta uvrB\ \Delta mfd,\ slow}$) of 24 ± 1 s (28 ± 2 %) (summarized in Fig. 3c; Supplementary Figure 2a-
148 b, and Table 1; error bars represent standard deviation of the bootstrap distribution of values obtained
149 by performing global fits to CRTDs ten times). To eliminate the possibility that this measured lifetime
150 is affected by cellular copy numbers of UvrA, we additionally created a strain that expresses *uvrA-YPet*
151 from its endogenous promoter, and lacks the genes for *uvrB* and *mfd* (*uvrA-YPet* Δ*uvrB* Δ*mfd*). The
152 measured lifetimes of UvrA-YPet in this strain were found to be identical within error ($\tau_{UvrA|uvrA\text{-}YPet}$

153 $_{\Delta uvrB\ \Delta mfd,\ \mathrm{slow}}$ = 22 ± 8 s (27 ± 4 %) and $\tau_{\mathrm{UvrA}|uvrA\text{-}YPet\ \Delta uvrB\ \Delta mfd,\ \mathrm{fast}}$ = 1.4 ± 0.4 s (73 ± 4%)) to those in the
154 Δ*uvrA* Δ*uvrB* Δ*mfd*/pUvrA-YPet strain (Fig. 3a and 3c, Supplementary Figure 2c-d and Table 1). Further,
155 we also measured the binding lifetime of a mutant UvrA that is deficient in its interactions with UvrB
156 and Mfd (Fig. 3b). Since UvrA interacts with both UvrB and Mfd *via* the interface formed by residues
157 131-250 [35, 36, 37], we expected that the labelled mutant UvrA lacking residues 131-250, UvrA(Δ131-
158 250)-YPet, would be a faithful reporter of binding of kinetics of UvrA alone in *uvrB*$^+$ *mfd*$^+$ cells (Fig. 3b).
159 Previous biochemical characterization of a UvrA(Δ131-248) mutant revealed that this mutant is unable
160 to interact with UvrB and catalyze TCR and GGR[22]. Indeed, interval imaging of UvrA(Δ131-250)-YPet
161 expressed from a low-copy plasmid (pUvrA(Δ131-250)-YPet) in Δ*uvrA* cells produced a binding lifetime
162 ($\tau_{\mathrm{UvrA}(\Delta 131-250)}$) of 29.7 ± 0.8 s (summarized in Fig. 3c, Supplementary Figure 2e-f, Table 1). It is
163 noteworthy that deletion of these residues leads to a complete abolishment of the short-lived species.
164 The reasons for this loss may lie in structural differences between the wild-type and mutant proteins.
165 Together, these results demonstrate that UvrA-YPet by itself is long-lived on DNA. Notably, the
166 lifetimes measured in our experiments reveal values that are larger than previous *in vitro*
167 measurements of UvrA binding[29]. The presence of two binding lifetimes reveals the presence of two
168 populations of UvrA on DNA.

169 **UvrB dissociates DNA-bound UvrA in cells lacking Mfd**

170 Next, we studied the influence of UvrB on the DNA binding lifetime of UvrA in cells lacking Mfd (*uvrA-*
171 *YPet* Δ*mfd* cells; Fig. 3d) during normal growth. In these cells, UvrA-YPet dissociated with a fast lifetime
172 ($\tau_{\mathrm{UvrA}|\ \Delta mfd,\ \mathrm{fast}}$) of 1.5 ± 0.1 s (amplitude: 78 ± 2%) and a slow lifetime ($\tau_{\mathrm{UvrA}|\ \Delta mfd,\ \mathrm{slow}}$) of 8.7 ± 0.4 s (22 ±
173 2%) (summarized in Fig. 3f; Supplementary Figure 2g-h, Table 1). The lifetime of the slowly dissociating
174 species observed in our measurements matches the lifetime detected for the dissociation of UvrA in
175 the presence of UvrB previously (7 s) [29], and is consistent with measurements of UvrB loading at sites
176 of DNA damage[38]. Notably, the fast lifetime is consistent with measurements from a previous study[23];
177 however, in this study a long-lived population of UvrA was not detected in the absence of exogenous
178 DNA damage[23].

179 Several *in vitro* studies have revealed that damage detection during NER proceeds *via* the loading of
180 UvrB on DNA, followed by damage verification mediated *via* the helicase activity of UvrB [39, 40, 41]. To
181 investigate whether the ability of UvrB to be loaded on DNA *via* its β-hairpin is essential for dissociation
182 of UvrA from DNA, we measured the lifetime of UvrA-YPet in *uvrA-YPet* Δ*mfd* cells expressing the β-
183 hairpin deletion mutant of UvrB from the native *uvrB* locus (Methods). This mutant, UvrB(ΔβHG), is
184 inefficiently loaded on DNA *in vitro* [42]. The lifetime ($\tau_{\mathrm{UvrA}|\ uvrB(\Delta\beta HG)\ \Delta mfd}$) of UvrA-YPet in cells expressing
185 UvrB(ΔβHG) from the chromosome was 148 ± 36 s (100%); over 15-fold longer than that of UvrA-YPet

186 in cells lacking Mfd (Fig. 3e-f, Supplementary Figure 2i-j and Table 1). These data indicate that the
187 UvrA-UvrB($\Delta\beta$HG) complex is arrested on DNA.

188 The lack of a short-lived species of UvrA in cells expressing mutant UvrB implies that the detectable
189 population of UvrA can be sequestered to the chromosome in the form of a long-lived complex. Such
190 a complex has been detected in single-molecule DNA stretching assays where UvrAB was
191 demonstrated to slide on DNA [29]. Additionally, we infer that in wild-type cells, loading of UvrB on DNA
192 must promote the dissociation of UvrA. Indeed, our single-molecule live-cell imaging results highlight
193 the physiological relevance of models constructed from *in vitro* studies that demonstrate that UvrB
194 facilitates the dissociation of UvrA from DNA [42, 43, 44]. These findings lead us to suggest that the 8.7s
195 lifetime measured here corresponds to the lifetime of UvrA engaged in damage surveillance activities,
196 where UvrA is turned over by UvrB loading.

197 **Mfd arrests UvrA on DNA in UvrB deficient cells**

198 Next, we measured the lifetime of UvrA in cells lacking UvrB in the absence of exogenous DNA damage.
199 Under these conditions, UvrA can form surveillance complexes ($UvrA_2$) and interact with Mfd engaged
200 with stalled RNAP. Interval imaging of UvrA-YPet in cells lacking UvrB (*uvrA-YPet* Δ*uvrB*) revealed a
201 single long-lived UvrA species with a lifetime ($\tau_{UvrA|\Delta uvrB}$) of 97 ± 18 s (Fig. 3g, Supplementary Figure
202 3a-b). Since UvrA alone binds DNA with a lifetime of approximately 24 s, this highly stable species must
203 reflect interactions with Mfd. We propose that this slowly dissociating species reflects the arrested
204 Mfd-UvrA complex[13] in cells lacking UvrB. Our attempts at co-localization of UvrA and Mfd using the
205 spectrally separated probes, YPet and PAmCherry, were limited by the poor expression of Mfd-
206 PAmCherry and UvrA-PAmCherry in cells under our standard growth conditions (Supplementary Note
207 1 and Supplementary Figure 3c-d). Considering the copy numbers of UvrA measured here (16 per cell)
208 and Mfd (22 per cell)[12], and the reported picomolar affinity of UvrA for Mfd[13], a large fraction of entire
209 population of UvrA can be efficiently sequestered in complex with Mfd, consistent with the
210 observation of only a single, slowly dissociating species in cells lacking *uvrB*.

211 **UvrA is longer lived on DNA in *mfd*$^+$ cells compared to *mfd*$^-$ cells in the absence of exogenous damage**

212 We next set out to measure the residence time of DNA-bound UvrA in cells carrying both Mfd and
213 UvrB in the absence of exogenous DNA damage. UvrA is recruited to DNA *via* Mfd to form the
214 asymmetric handoff complex Mfd-$UvrA_2$-UvrB that couples failed TECs to the repair machinery, unlike
215 the symmetric UvrB-$UvrA_2$-UvrB complex formed during damage surveillance in the absence of Mfd
216 (Fig. 1). Our previous characterization of Mfd demonstrated that the residence time of Mfd is
217 governed by UvrA, suggesting that UvrA is recruited to Mfd during normal growth[12]. Hence, we

218 anticipated three scenarios for the lifetime of UvrA in wild-type cells. First, if the residence time of
219 UvrA-YPet is equal to 8.7 s, this would indicate either that the lifetimes of Mfd-UvrA and UvrA-UvrB
220 interactions are similar, or that the lifetimes are different but the recruitment of UvrAB to RNAP-
221 bound Mfd occurs so infrequently that only UvrAB complexes are detected. Second, a lifetime shorter
222 than 8.7 s would suggest that Mfd promotes the dissociation of UvrA. Finally, a lifetime longer than
223 8.7 s would indicate that Mfd stabilizes UvrA.

224 To distinguish between these three scenarios, we imaged UvrA-YPet in wild-type cells. Interval imaging
225 of UvrA-YPet revealed a short-lived species with a lifetime ($\tau_{UvrA,\ fast}$) of 1.9 ± 0.2 s (79 ± 0.2%) and a
226 long-lived species of UvrA with a lifetime ($\tau_{UvrA,\ slow}$) of 12.0 ± 0.8 s (21 ± 2%) (Fig. 4a, b, Supplementary
227 Figure 4a-b, Table 1). To identify whether this lifetime reflected Mfd-dependent or independent
228 interactions, we imaged *uvrA-YPet* cells in conditions where Mfd-RNAP interactions are abolished by
229 rifampicin (rif) treatment. Interval imaging of UvrA-YPet in rif-treated cells revealed a short-lived
230 species with a lifetime ($\tau_{UvrA|rif,fast}$) of 1.5 ± 0.3 s (63 ± 3 %) and a long-lived species of UvrA-YPet
231 possessing a lifetime ($\tau_{UvrA|rif,\ slow}$) of 9.6 ± 0.6 s (37 ± 3 %) (Fig. 4a, c, Supplementary Figure 4c-d, Table
232 1). As expected, the slow lifetime of UvrA-YPet in rif-treated cells matches that in cells lacking Mfd.
233 Further, measurements of UvrA-YPet fluorescence in rif-treated cells did not reveal a loss of YPet
234 fluorescence arising from enhanced degradation of UvrA-YPet upon rif treatment (Supplementary
235 Figure 4i). The decrease in the long-lived lifetime from 12.0 s to 9.6 s indicates that a slowly dissociating
236 species (lifetime greater than 8.7 s) of UvrA is lost upon rif treatment, one that is involved in Mfd-
237 dependent interactions. These results lead us to conclude that the interactions of Mfd-UvrAB
238 complexes are more stable than UvrAB complexes alone.

239 Since no mutants of UvrA have been identified that exclusively form the Mfd-$UvrA_2$-UvrB complex but
240 not the $UvrA_2UvrB_2$ complex in cells, measurement of the lifetime of UvrA in the Mfd-$UvrA_2$-UvrB
241 complex is difficult. Nevertheless, it is conceivable that the lifetime of the Mfd-$UvrA_2$-UvrB complex
242 could be influenced by the availability of downstream factors including UvrAB. We tested this
243 hypothesis by measuring the lifetime of UvrA-YPet in wild-type cells expressing UvrA-YPet from the
244 plasmid (Δ*uvrA*/pUvrA-YPet). Since UvrA can engage UvrB in solution, we reasoned that higher
245 expression levels of UvrA would bind UvrB to form the $UvrA_2B_2$ surveillance complex, leaving little free
246 UvrB for engagement with Mfd-$UvrA_2$ complexes. Consistent with this expectation, the data revealed
247 a short-lived species with a lifetime ($\tau_{UvrA|\uparrow,\ fast}$) of 2.0 ± 0.1 s (74 ± 2 %) and a previously unencountered
248 population of long-lived UvrA possessing a lifetime ($\tau_{UvrA|\uparrow,\ slow}$) of 19 ± 1 s (26 ± 2%) (Fig. 4a, d,
249 Supplementary Figure 4e-f, Table 1).

250 In cells, UvrA is involved in target search (1.6 ± 0.1 s and 24 ± 1 s lifetimes, Fig. 3c) and damage
251 surveillance as part of $UvrA_2B_2$ (8.7 s lifetime, Fig. 3f) in addition to Mfd-dependent UvrA(B) complexes
252 (with lifetime of at least 12 s). To identify whether this long-lived UvrA species (19 ± 1 s lifetime)
253 interacts with Mfd, we treated Δ*uvrA*/pUvrA-YPet cells with rifampicin. Under this condition, we
254 expected to recover the lifetime of UvrA as part of $UvrA_2$ or $UvrA_2B_2$ complexes. Indeed,
255 measurements of lifetimes of UvrA-YPet in rif-treated Δ*uvrA*/pUvrA-YPet cells revealed a lifetime
256 ($\tau_{UvrA|\uparrow rif,\ slow}$) of 11.5 ± 0.6 s (25 ± 2%) and a short lifetime ($\tau_{UvrA|\uparrow rif,\ fast}$) of 1.7 ± 0.1 s (75 ± 2%) (Fig. 4a,
257 e, Supplementary Figure 4g-h, Table 1). The faster turnover of UvrA in response to rif treatment is
258 consistent with the inference that the lifetime of UvrA in the Mfd-$UvrA_2$-UvrB intermediate is longer
259 than that in the $UvrA_2B_2$ intermediate in the absence of exogenous damage.

260 Notably, rif treatment of Δ*uvrA*/pUvrA-YPet cells yielded a lifetime (11.5 s) that is longer than that
261 measured for rif-treated *uvrA-YPet* cells (9.6 s), and cells lacking *mfd* (8.7 s). The simplest explanation
262 consistent with these observations is that under conditions of high relative UvrA/UvrB abundance the
263 population is composed of $UvrA_2B_{(2)}$ complexes (lifetime of 8.7 s) and DNA-bound $UvrA_2$ awaiting
264 turnover by UvrB (lifetime of 24 s). We suggest that at higher cellular concentrations of UvrA relative
265 to UvrB and Mfd, the existing population of UvrB is now required to turnover a greater number of
266 UvrA molecules on undamaged DNA and at sites of endogenous damage, in addition to TCR
267 intermediates. This model predicts that Mfd and UvrA must form a TCR intermediate whose
268 disassembly is contingent on the arrival of UvrB. Together these results highlight two important
269 features of prokaryotic NER: first, that damage surveillance by UvrA is highly dynamic and can be
270 readily diverted from one pathway to the other depending on the condition, and second that the
271 lifetime of individual actors is determined by the presence of downstream factors.

272 **UvrA-Mfd interactions are prioritized in cells after UV irradiation**

273 Next, we set out to characterize the behaviour of the UvrA in response to DNA damage. UV irradiation
274 leads to the formation of UV-induced lesions in the chromosome[45]. These in turn elicit the induction
275 of the SOS response during which the expression of UvrA and UvrB are upregulated[46]. The elevated
276 levels of UvrA promote rapid removal of UV lesions from the DNA. To quantify this SOS-induced
277 upregulation in real time, we set out to monitor the relative abundance of UvrA in cells following UV
278 irradiation.

279 Time-lapse experiments on UV-irradiated *uvrA-YPet* allowed us to monitor the cellular fluorescence
280 of tagged UvrA as a function of time. We immobilized *uvrA-YPet* cells in a flow cell with a quartz
281 window and delivered a dose of 20 Jm^{-2} of damaging 254-nm UV light (Fig. 5a). This was followed by

282 acquiring a single snapshot upon laser illumination with 514-nm light, every five minutes for three
283 hours. Quantification of cellular fluorescence intensities revealed that the integrated fluorescence
284 intensities of single *uvrA-YPet* cells increase 30 minutes after UV exposure by three-fold, consistent
285 with the rapid deregulation of the SOS inducible *uvrA* promoter (Fig. 5b)[47, 48]. UvrA copy numbers have
286 been suggested to increase from 25 to 250 copies per cell after SOS induction[49]. We note that since
287 the experimental conditions associated with these measurements are not available in the published
288 literature, we are unable to effectively compare our measurements with these numbers.
289 Nevertheless, the basal levels and the exact extent of fold-induction after SOS induction may depend
290 on the nature and dosage of the genotoxin, as well as growth conditions such as medium and
291 temperature. Consistent with this argument, the copy numbers of UvrA were found to rise six-fold
292 within 40 minutes of UV exposure (40 Jm^{-2}) in cells growing at 37 °C in previous work [50].

293 Since UV-induced lesions are a substrate for UvrAB (reviewed in ref. [1]), we then set out to measure
294 the lifetime of UvrA in UV-irradiated cells. To that end, we irradiated TCR-deficient cells (*uvrA-YPet*
295 Δ*mfd*) with a pulse of 254-nm UV light delivered *in situ*. This was followed by interval imaging in four
296 rounds, each lasting 25 minutes. Analysis of the complete data set revealed binding kinetics of UvrA-
297 YPet corresponding to a short-lived species with a lifetime ($\tau_{UvrA|\ \Delta mfd,\ UV\ fast}$) of 1.6 ± 0.1 s (77 ± 3%) and
298 a long-lived species of UvrA corresponding to a lifetime of ($\tau_{UvrA|\ \Delta mfd,\ UV\ slow}$) 13.1 ± 0.6 s (23 ± 2%) (Fig.
299 5c, and Supplementary Figure 5, Table 1). Strikingly the lifetime of the slowly dissociating species was
300 larger than that detected in the absence of exogeneous DNA damage (8.7 s).

301 Seeking an explanation for the increase in binding lifetime of UvrA-YPet following UV exposure, we
302 wondered if the longer lifetime of UvrA detected in these experiments represented temporally
303 averaged measurements. Since each set of interval measurements lasted 25 min, we proceeded to
304 disaggregate each data set into the four constitutive 25-min intervals after UV exposure. Analysis of
305 the resulting data from each time window revealed that the measured lifetime of UvrA changes as a
306 function of the experimental timeline after the UV pulse (Fig. 5c, and Supplementary Fig. 5, Table 1).
307 Indeed, in the first 25 minutes, the slow lifetime of UvrA (9.6 ± 1 s) matched that measured in the
308 absence of DNA damage (8.7 ± 0.4 s). This lifetime increased to a maximum of 15 ± 2 s in the 50-75
309 minute time window, finally plateauing to 15 ± 4 s in the 75-100 minute time window after UV
310 exposure.

311 There are two main takeaways from these experiments. First, the lifetime of short-lived UvrA does not
312 change upon UV exposure, and is identical to that measured in the absence of any exogenous DNA
313 damage. We therefore conclude that this species is involved in binding undamaged DNA. Second, since

314 the lifetime of long-lived UvrA changes upon UV exposure, we conclude that this species is engaged
315 in DNA damage recognition.

316 Next, we repeated the interval imaging experiments on wild-type cells (*uvrA-YPet*) following exposure
317 to a 20 Jm^{-2} pulse of 254-nm UV light provided *in situ*. In this case, UvrA-YPet exhibited two kinetic
318 populations after UV-exposure, a short-lived population with a lifetime of 1.5 ± 0.1 s (74 ± 2 %) and a
319 second, longer lived population with a lifetime of 9.9 ± 0.4 s (26 ± 2%) (Fig. 5d, and Supplementary
320 Figure 6, Table 1). As before, we disaggregated each data set into the four constitutive 25-min intervals
321 after UV exposure. In contrast to TCR-deficient cells, the measured lifetime of UvrA in wild-type cells
322 remained low (8.4 ± 0.6 s) in the 75-100 minute time window after UV exposure. These data indicate
323 that UvrA is turned over faster in an Mfd-dependent manner during the SOS response.

324 Next, we plotted the amplitude of the long lived species in each time-window after UV irradiation
325 (Figure 5e). In *uvrA-YPet* cells, the fraction of the population dissociating with a slow off rate was
326 greatest in the first 50 minutes after UV exposure (at approximately 30%), and subsequently dropped
327 rapidly to 13 ± 2% at 100 minutes after UV. In comparison, *uvrA-YPet* Δ*mfd* cells exhibited a non-linear
328 trajectory that nevertheless exhibited a similar reduction in the fraction of UvrA-YPet possessing a
329 slow off rate. The most striking difference between the two strains was apparent at the 50 minute
330 time point – cells carrying *mfd* exhibited a 1.5-fold greater fraction of UvrA molecules dissociating with
331 the slow lifetime. These results are broadly consistent with the expectation that as repair progresses,
332 fewer unrepaired lesions are available for UvrA to bind to.

333 We followed these studies with an investigation of the binding lifetimes of Mfd. In the absence of
334 exogenous DNA damage, the lifetime of Mfd is approximately 18 s[12]. Interval imaging of Mfd-YPet in
335 *mfd-YPet* cells exposed to UV light revealed that the lifetime of Mfd-YPet dropped during the course
336 of the SOS response, leading to an average lifetime ($\tau_{Mfd|UV}$) of 12 s (Fig. 5d, and Supplementary Figure
337 7, Table 1). Strikingly, the binding lifetime of Mfd mirrored that of UvrA in wild-type cells in the time
338 window from 25-100 min after UV, providing further evidence in support of an Mfd-UvrA complex in
339 cells.

340 **Discussion**

341 UvrA is the central player in NER since it performs critical functions in both GGR and TCR: First, it
342 recognizes DNA damage as $UvrA_2$ or $UvrA_2B_{(2)}$ and loads UvrB in GGR and second, it stimulates TCR by
343 interacting with Mfd.

344 In this work, we set out to visualize the binding behaviour of fluorescently tagged UvrA in living cells
345 over the experimentally accessible, and biologically relevant timescale of 0.1 – 1000 s. We found that
346 in live cells, UvrA exhibits foci with residence times ranging from a few hundred milliseconds, to tens
347 of seconds. Here, using single-molecule imaging in combination with chemical and genetic tools, we
348 characterized the DNA-binding lifetimes of UvrA in its interactions with its key binding partners in live
349 cells.

350 We identified that UvrA is long-lived on DNA in the absence of Mfd and UvrB with a lifetime of 24 s.
351 Consistent with previous studies demonstrating that UvrB promotes the dissociation of UvrA *in vitro*,
352 UvrA also dissociated faster in *uvrB*$^+$ cells [42, 43, 44]. The insensitivity to rif or UV treatment suggests that
353 the short-lived population of DNA-bound UvrA with a lifetime of ~2 s corresponds to UvrA engaged in
354 damage search. Additionally, we also detected a long-lived species of UvrA in untreated cells. Using
355 TCR-deficient strains and rif treatment, we assigned the lifetime of UvrA in interactions with UvrB to
356 be 8.7 s. This lifetime likely corresponds to UvrA dissociation following loading of UvrB on DNA since
357 the loading-deficient UvrB mutant arrests UvrA for 148 s (see Fig. 3). Overall, our findings are
358 consistent with a previous study that detected a short-lived UvrA species in untreated cells, and a
359 long-lived species upon UV treatment [23].

360 Three observations provide evidence for an Mfd-UvrA interaction in cells: first, cells lacking UvrB
361 exhibited UvrA-YPet foci that were five-fold longer lived compared to cells lacking both Mfd and UvrB,
362 suggesting that UvrA forms a highly stable complex with Mfd. Second, the long-lived lifetime of UvrA
363 in non-UV treated cells was sensitive to rif treatment, whereby these cells lost a slowly dissociating
364 species of UvrA upon rif treatment, presumably engaged with Mfd. Curiously, the DNA binding kinetics
365 of UvrA in Mfd-$UvrA_2$-UvrB complexes could only be distinguished from those in $UvrA_2B_2$ under
366 conditions where UvrB was present in limiting conditions, suggesting a role for UvrB in resolving Mfd-
367 UvrA complexes in cells (Fig. 5f). A prediction of this hypothesis is that elevated concentrations of UvrB
368 would lead to an enhanced turnover of Mfd in the Mfd-$UvrA_2$-UvrB complex. Third, experiments on
369 cells exposed to UV light revealed that the binding kinetics of UvrA mirrored those of Mfd suggesting
370 that these two proteins participate in a TCR handoff complex during the SOS response. Further, UvrA
371 is turned over faster in an Mfd-dependent manner during the SOS response compared to untreated
372 cells (Fig. 5). The elevated copy numbers of UvrA and UvrB following UV treatment (Fig. 5b and refs [47,
373 48]) may explain the faster turnover of UvrA during the SOS response.

374 The lifetime of UvrA in TCR-deficient UV-treated cells increased to 15 s, but remained low in UV-
375 treated wild-type cells. An explanation for this striking difference may be found in work by Crowley
376 and Hanawalt [46]. The differences observed in our experiments may fundamentally be attributable to

377 the efficiencies with which UvrA recognizes CPDs and 6-4 photoproducts. CPD lesions[51, 52] being less
378 helix distorting than 6-4 photoproducts[53, 54], are generally inefficiently recognized by damage
379 recognition enzymes in NER across organisms[55, 56]. CPD recognition by RNA polymerase and
380 subsequent TCR at such sites is a major mechanism for CPD removal after UV treatment[46]. Compared
381 to untreated cells that remove greater than 80% of CPD lesions within 40 minutes following UV
382 treatment, rif-treated cells removed less than 50% of CPD lesions at the same time point[46]. In contrast,
383 6-4 photoproduct removal was uninfluenced by rif treatment[46]. Further, this report also demonstrated
384 that the copy number of UvrAB determines whether CPDs are efficiently removed following UV
385 treatment. Considering the low expression level of UvrA-YPet in our strain (16 ± 4 subunits per cell
386 during normal growth), it is likely that the initial time window in which UvrA is turned over rapidly in
387 Δ*mfd* cells reflects repair of 6-4 photoproducts. The later time windows in which UvrA exhibits a
388 lifetime of 15 s may reflect repair of CPD lesions that are poorly detected by UvrA. Extending this
389 argument, the prediction from the Crowley and Hanawalt study is that the rapid turnover of UvrA in
390 wild-type cells in the 25-100 min time window reflects the repair of CPDs *via* TCR. Indeed, consistent
391 with this prediction, we found that the binding kinetics of Mfd mirror those of UvrA in this time period.
392 This finding is also consistent with the well-established finding that the repair of UV lesions is biphasic
393 – a period of rapid removal of 6-4 photoproducts is followed by a slower repair of CPDs[46].

394 Finally, our data suggest that the enhancement of the rate of repair in TCR *vs*. GGR measured in bulk
395 is best explained by enhanced target search in TCR compared to GGR. This model has been previously
396 proposed in the literature based on evidence from *in vitro* studies[6, 13]. In this model, stalled RNAP is
397 recognized by Mfd, leading to the exposure of Mfd's UvrB-homology module (BHM) that in turn acts
398 as an 'flag' for UvrAB. Damage recognition by UvrAB would then follow initial recruitment to the site
399 of the lesion. In contrast, target search during global genomic repair would comprise of repeated
400 cycles of 3D diffusion of UvrA(B) to sites of undamaged DNA followed by subsequent turn-over of UvrA
401 by UvrB until the damage surveillance complex stochastically encounters damaged DNA.

402

403

404 **METHODS**

405 **Construction of strains and plasmids**

406 *Escherichia coli* MG1655 *uvrA-YPet* was constructed using λ Red recombination as previously
407 described for Mfd using the linker sequence described previously[12]. Deletion constructs were created
408 by replacing the indicated gene with a kanamycin cassette flanked by FRT sites as described
409 previously[12]. Sequence specified wild-type *uvrA* and *uvrA*(Δ131-250) geneblocks (including the native
410 *uvrA* promoter) were ordered from IDT (Coralville, USA) and subcloned into pHH001[12] using standard
411 molecular biology techniques. Plasmids were sequenced on both strands prior to use. Strain
412 expressing mutant UvrB was created using CRISPR-Cas9 assisted λ Red recombination as previously
413 described[57, 58] (see Supplementary Methods).

414 **Cell culture for imaging**

415 Cells were imaged in quartz-top flow cells as described previously[12]. Cells were grown in 500 µL of EZ-
416 rich defined media (Teknova, CA, US), supplemented with 0.2% (v/v) glucose in 2 mL microcentrifuge
417 tubes at 30 °C. For experiments involving plasmid-expressed UvrA-YPet or UvrA(Δ131-250)-YPet,
418 spectinomycin (50 µg per mL) was added to the growth media. Cells in early exponential phase were
419 loaded in flow cells at 30 °C, followed by a constant supply of aerated EZ-rich defined media at a rate
420 of 30 µL per min, using a syringe pump (Adelab Scientific, Australia).

421 **Single-molecule live-cell imaging**

422 Single-molecule fluorescence imaging was carried out with a custom-built microscope as previously
423 described[12]. Briefly, the microscope comprised a Nikon Eclipse Ti body, a 1.49 NA 100x objective, a
424 514-nm Sapphire LP laser (Coherent) operating at a power density of 71 W cm^{-2}, an ET535/30m
425 emission filter (Chroma) and a 512 x 512 $pixel^2$ EM-CCD camera (either Photometrics Evolve or Andor
426 iXon 897). The microscope was operated in near-TIRF illumination[59] and was controlled using NIS-
427 Elements (Nikon). PAmCherry-tagged proteins were imaged as described previously[12].

428 Fluorescence images were acquired in time-series format with 100 ms frames. Each video acquisition
429 contained two phases. The first phase (50 frames) aimed to lower background signal by continuous
430 illuminating, causing most of the fluorophores to photo-bleach or to assume a dark state. The second
431 phase (single-molecule phase lasting for 100 frames) is when single molecules can be reliably tracked
432 on a low background signal. In the second phase, consecutive frames were acquired continuously or
433 with a delay time (τ_d).

434 **Image analysis**

435 Image analysis was performed in Fiji[60], using the Single Molecule Biophysics plugins (available at
436 https://github.com/SingleMolecule/smb-plugins), and MATLAB. First, raw data were converted to TIF
437 format, following by background correction and image flattening as previously described[12]. Next, foci
438 were detected in the reactivation phase by applying a discoidal average filter (inner radius of one pixel,
439 outer radius of three pixels), then selecting pixels above the intensity threshold. Foci detected within
440 3-pixel radius (318 nm) in consecutive frames were considered to belong to the same binding event.

441 **Interval imaging for dissociation kinetics measurements**

442 Interval imaging was performed as described previously[12]. Briefly, the photobleaching phase
443 contained 50 continuous 0.1-s frames. In phase II, 100 discontinuous 0.1-s frames (τ_{int} = 0.1 s) were
444 collected with time-lapse time (τ_{tl}) ranging from τ_{tl} = (0.1, 0.2, 0.5, 1, 2, 4, 8, 10). In each experiment,
445 videos with varying τ_d were acquired. Foci were detected using a relative intensity threshold of 7 or 8
446 above the background as appropriate. Depending on the construct being imaged, between 3-15
447 repeats of each experiment were collected for each strain. Cumulative residence time distribution of
448 binding events detected in all data sets were generated for each τ_{tl}. Cumulative residence time
449 distributions were globally fitting to single- or double-exponential models to obtain binding lifetimes
450 and amplitudes of kinetic subpopulations (custom-written MATLAB codes, see ref. [24]). Here, the choice
451 of fitting model was decided based on the shape of $k_{eff}\tau_{tl}$ vs. τ_{tl} plot (ref.[32]), in which the effective decay
452 rate k_{eff} represents the sum of the normalized photobleaching rate k_b and the off rate k_{off} ($k_{eff} = k_b\tau_{int}$
453 $/\tau_{tl} + k_{off}$) (ref. 32). The linearity of $k_{eff}\tau_{tl}$ vs. τ_{tl} plot represents a single kinetic population whereas
454 deviations from linear fits indicate multiple kinetic subpopulations (ref. 32). The corresponding $k_{eff}\tau_{tl}$
455 vs. τ_{tl} plot was obtained as described previously[12, 24], with the shaded error bar representing standard
456 deviations of ten bootstrapped samples deriving from 80% of the compiled binding events (custom-
457 written MATLAB codes)[24]. Given that this method is based on fitting mixtures of exponential models
458 to the data, this approach reliably resolves off rates that are at least three-fold apart. In experiments
459 involving rifampicin treatment, cells were incubated in growth media containing rifampicin (50 µg per
460 mL) for 30 min in the flow cell prior to imaging.

461 **Experiments involving UV irradiation**

462 UV survival assays were performed as described previously in references[12, 61]. UV irradiation was
463 delivered *in situ* as described previously[61]. The UV flux was measured prior to UV irradiation, and the
464 exposure time was adjusted to provide a dose of 20 Jm^{-2}. For experiments involving interval imaging

465 following UV exposure, τ_{tl} = (0.1, 0.3, 1, 3, 10) values were used to minimize the time taken to complete
466 one round of interval imaging.

467 **ACKNOWLEDGEMENTS**

468 H.G. acknowledges the University of Wollongong and the Faculty of Science, Medicine and Health for
469 funding of the Andor iXon 897 used in this work. A.M. van Oijen would like to acknowledge support
470 by the Australian Research Council (DP150100956 and FL140100027).

471 **AUTHOR CONTRIBUTIONS**

472 Construct creation: H.G. and H.N.H.; Data curation: H.G.; Data analysis: H.G. and H.N.H.; Software:
473 H.N.H. and H.G.; Writing—Original draft: H.G.; Writing—review and editing: H.N.H., H.G. and A.M.v.O.;
474 Conceptualization: H.G.; Supervision: H.G. and A.M.v.O.

475 **Competing interests**

476 The authors declare no competing interests.

477 **Materials and Correspondence**

478 Harshad Ghodke, Molecular Horizons and School of Chemistry and Molecular Bioscience, University
479 of Wollongong, Wollongong, New South Wales, 2522, Australia

480 **Data availability**

481 The data that support the findings of this study are available from the corresponding author upon
482 reasonable request.

483 **Code availability**

484 Custom code used for data analyses has been made publicly available at
485 github.com/hghodke/bacterial_live_cell_interval_imaging

486 **References**

487 1. Van Houten B. Nucleotide excision repair in Escherichia coli. *Microbiol Rev* **54**, 18-51 (1990).

488
489 2. Kisker C, Kuper J, Van Houten B. Prokaryotic nucleotide excision repair. *Cold Spring Harb*
490 *Perspect Biol* **5**, a012591 (2013).

491
492 3. Scharer OD. Nucleotide excision repair in eukaryotes. *Cold Spring Harb Perspect Biol* **5**,
493 a012609 (2013).

494
495 4. Romano V, Napoli A, Salerno V, Valenti A, Rossi M, Ciaramella M. Lack of strand-specific
496 repair of UV-induced DNA lesions in three genes of the archaeon Sulfolobus solfataricus. *J*
497 *Mol Biol* **365**, 921-929 (2007).

498
499 5. Dorazi R, Gotz D, Munro S, Bernander R, White MF. Equal rates of repair of DNA
500 photoproducts in transcribed and non-transcribed strands in Sulfolobus solfataricus. *Mol*
501 *Microbiol* **63**, 521-529 (2007).

502
503 6. Hanawalt PC, Spivak G. Transcription-coupled DNA repair: two decades of progress and
504 surprises. *Nat Rev Mol Cell Biol* **9**, 958-970 (2008).

505
506 7. Xu J*, et al.* Structural basis for the initiation of eukaryotic transcription-coupled DNA repair.
507 *Nature* **551**, 653-657 (2017).

508
509 8. Deaconescu AM, Darst SA. Crystallization and preliminary structure determination of
510 Escherichia coli Mfd, the transcription-repair coupling factor. *Acta Crystallogr Sect F Struct*
511 *Biol Cryst Commun* **61**, 1062-1064 (2005).

512
513 9. Selby CP, Sancar A. Molecular mechanism of transcription-repair coupling. *Science* **260**, 53-
514 58 (1993).

515
516 10. Selby CP, Sancar A. Transcription-repair coupling and mutation frequency decline. *Journal of*
517 *bacteriology* **175**, 7509-7514 (1993).

518
519 11. Selby CP, Witkin EM, Sancar A. Escherichia coli mfd mutant deficient in "mutation frequency
520 decline" lacks strand-specific repair: in vitro complementation with purified coupling factor.
521 *Proc Natl Acad Sci U S A* **88**, 11574-11578 (1991).

522
523 12. Ho HN, van Oijen AM, Ghodke H. The transcription-repair coupling factor Mfd associates
524 with RNA polymerase in the absence of exogenous damage. *Nat Commun* **9**, 1570 (2018).

525
526 13. Fan J, Leroux-Coyau M, Savery NJ, Strick TR. Reconstruction of bacterial transcription-
527 coupled repair at single-molecule resolution. *Nature* **536**, 234-237 (2016).

528
529 14. Sarker AH*, et al.* Recognition of RNA polymerase II and transcription bubbles by XPG, CSB,
530 and TFIIH: insights for transcription-coupled repair and Cockayne Syndrome. *Mol Cell* **20**,
531 187-198 (2005).

532
533 15. Mellon I, Spivak G, Hanawalt PC. Selective removal of transcription-blocking DNA damage
534 from the transcribed strand of the mammalian DHFR gene. *Cell* **51**, 241-249 (1987).

535
536 16. Sweder KS, Hanawalt PC. Preferential repair of cyclobutane pyrimidine dimers in the
537 transcribed strand of a gene in yeast chromosomes and plasmids is dependent on
538 transcription. *Proc Natl Acad Sci U S A* **89**, 10696-10700 (1992).

539
540 17. Ganesan AK, Hanawalt PC. Transcription-coupled nucleotide excision repair of a gene
541 transcribed by bacteriophage T7 RNA polymerase in Escherichia coli. *DNA Repair (Amst)* **9**,
542 958-963 (2010).

543
544 18. Mellon I, Hanawalt PC. Induction of the Escherichia coli lactose operon selectively increases
545 repair of its transcribed DNA strand. *Nature* **342**, 95-98 (1989).

546
547 19. Bohr VA, Smith CA, Okumoto DS, Hanawalt PC. DNA repair in an active gene: removal of
548 pyrimidine dimers from the DHFR gene of CHO cells is much more efficient than in the
549 genome overall. *Cell* **40**, 359-369 (1985).

550
551 20. Smerdon MJ, Thoma F. Site-specific DNA repair at the nucleosome level in a yeast
552 minichromosome. *Cell* **61**, 675-684 (1990).

553
554 21. Howan K*, et al.* Initiation of transcription-coupled repair characterized at single-molecule
555 resolution. *Nature* **490**, 431-434 (2012).

556
557 22. Manelyte L, Kim YI, Smith AJ, Smith RM, Savery NJ. Regulation and rate enhancement during
558 transcription-coupled DNA repair. *Mol Cell* **40**, 714-724 (2010).

559
560 23. Stracy M*, et al.* Single-molecule imaging of UvrA and UvrB recruitment to DNA lesions in
561 living Escherichia coli. *Nat Commun* **7**, 12568 (2016).

562
563 24. Ho HN, Zalami, D., Köhler, J., van Oijen, A.M., Ghodke, H. Identifying multiple kinetic
564 populations of DNA binding proteins in live cells using single-molecule fluorescence imaging.
565 *bioRxiv*, (2019).

566
567 25. Truglio JJ*, et al.* Structural basis for DNA recognition and processing by UvrB. *Nat Struct Mol*
568 *Biol* **13**, 360-364 (2006).

569

570 26. Croteau DL, DellaVecchia MJ, Wang H, Bienstock RJ, Melton MA, Van Houten B. The C-
571 terminal zinc finger of UvrA does not bind DNA directly but regulates damage-specific DNA
572 binding. *J Biol Chem* **281**, 26370-26381 (2006).

573
574 27. Nguyen AW, Daugherty PS. Evolutionary optimization of fluorescent proteins for intracellular
575 FRET. *Nat Biotechnol* **23**, 355-360 (2005).

576
577 28. Datsenko KA, Wanner BL. One-step inactivation of chromosomal genes in Escherichia coli K-
578 12 using PCR products. *Proc Natl Acad Sci U S A* **97**, 6640-6645 (2000).

579
580 29. Kad NM, Wang H, Kennedy GG, Warshaw DM, Van Houten B. Collaborative dynamic DNA
581 scanning by nucleotide excision repair proteins investigated by single- molecule imaging of
582 quantum-dot-labeled proteins. *Mol Cell* **37**, 702-713 (2010).

583
584 30. Schmidt A*, et al.* The quantitative and condition-dependent Escherichia coli proteome. *Nat*
585 *Biotechnol* **34**, 104-110 (2016).

586
587 31. Churchward G, Belin D, Nagamine Y. A pSC101-derived plasmid which shows no sequence
588 homology to other commonly used cloning vectors. *Gene* **31**, 165-171 (1984).

589
590 32. Gebhardt JC*, et al.* Single-molecule imaging of transcription factor binding to DNA in live
591 mammalian cells. *Nat Methods* **10**, 421-426 (2013).

592
593 33. Liao Y, Li Y, Schroeder JW, Simmons LA, Biteen JS. Single-Molecule DNA Polymerase
594 Dynamics at a Bacterial Replisome in Live Cells. *Biophys J* **111**, 2562-2569 (2016).

595
596 34. Hipp L*, et al.* Single-molecule imaging of the transcription factor SRF reveals prolonged
597 chromatin-binding kinetics upon cell stimulation. *Proc Natl Acad Sci U S A* **116**, 880-889
598 (2019).

599
600 35. Pakotiprapha D*, et al.* Crystal structure of Bacillus stearothermophilus UvrA provides insight
601 into ATP-modulated dimerization, UvrB interaction, and DNA binding. *Mol Cell* **29**, 122-133
602 (2008).

603
604 36. Pakotiprapha D, Samuels M, Shen K, Hu JH, Jeruzalmi D. Structure and mechanism of the
605 UvrA-UvrB DNA damage sensor. *Nat Struct Mol Biol* **19**, 291-298 (2012).

606
607 37. Deaconescu AM, Sevostyanova A, Artsimovitch I, Grigorieff N. Nucleotide excision repair
608 (NER) machinery recruitment by the transcription-repair coupling factor involves unmasking
609 of a conserved intramolecular interface. *Proc Natl Acad Sci U S A* **109**, 3353-3358 (2012).

610
611 38. Orren DK, Sancar A. Formation and enzymatic properties of the UvrB.DNA complex. *J Biol*
612 *Chem* **265**, 15796-15803 (1990).

613
614 39. Malta E, Moolenaar GF, Goosen N. Dynamics of the UvrABC nucleotide excision repair
615 proteins analyzed by fluorescence resonance energy transfer. *Biochemistry* **46**, 9080-9088
616 (2007).

617
618 40. Orren DK, Sancar A. The (A)BC excinuclease of Escherichia coli has only the UvrB and UvrC
619 subunits in the incision complex. *Proc Natl Acad Sci U S A* **86**, 5237-5241 (1989).

620
621 41. Lin JJ, Sancar A. (A)BC excinuclease: the Escherichia coli nucleotide excision repair enzyme.
622 *Mol Microbiol* **6**, 2219-2224 (1992).

623
624 42. Skorvaga M, Theis K, Mandavilli BS, Kisker C, Van Houten B. The beta -hairpin motif of UvrB
625 is essential for DNA binding, damage processing, and UvrC-mediated incisions. *J Biol Chem*
626 **277**, 1553-1559 (2002).

627
628 43. Skorvaga M*, et al.* Identification of residues within UvrB that are important for efficient DNA
629 binding and damage processing. *J Biol Chem* **279**, 51574-51580 (2004).

630
631 44. DellaVecchia MJ, Croteau DL, Skorvaga M, Dezhurov SV, Lavrik OI, Van Houten B. Analyzing
632 the handoff of DNA from UvrA to UvrB utilizing DNA-protein photoaffinity labeling. *J Biol*
633 *Chem* **279**, 45245-45256 (2004).

634
635 45. Rastogi RP, Richa, Kumar A, Tyagi MB, Sinha RP. Molecular mechanisms of ultraviolet
636 radiation-induced DNA damage and repair. *J Nucleic Acids* **2010**, 592980 (2010).

637
638 46. Crowley DJ, Hanawalt PC. Induction of the SOS Response Increases the Efficiency of Global
639 Nucleotide Excision Repair of Cyclobutane Pyrimidine Dimers, but Not 6-4 Photoproducts, in
640 UV-Irradiated Escherichia coli. *Journal of Bacteriology* **180**, 3345-3352 (1998).

641
642 47. Courcelle J, Khodursky A, Peter B, Brown PO, Hanawalt PC. Comparative gene expression
643 profiles following UV exposure in wild-type and SOS-deficient Escherichia coli. *Genetics* **158**,
644 41-64 (2001).

645
646 48. Kenyon CJ, Walker GC. Expression of the E. coli uvrA gene is inducible. *Nature* **289**, 808-810
647 (1981).

648
649 49. Selby CP, Sancar A. Structure and function of the (A)BC excinuclease of Escherichia coli.
650 *Mutat Res* **236**, 203-211 (1990).

651
652 50. Crowley DJ, Hanawalt PC. Induction of the SOS response increases the efficiency of global
653 nucleotide excision repair of cyclobutane pyrimidine dimers, but not 6-4 photoproducts, in
654 UV-irradiated Escherichia coli. *Journal of bacteriology* **180**, 3345-3352 (1998).

655

656 51. Park H*, et al.* Crystal structure of a DNA decamer containing a cis-syn thymine dimer. *Proc*
657 *Natl Acad Sci U S A* **99**, 15965-15970 (2002).

658
659 52. Husain I, Griffith J, Sancar A. Thymine dimers bend DNA. *Proc Natl Acad Sci U S A* **85**, 2558-
660 2562 (1988).

661
662 53. Kim JK, Choi BS. The solution structure of DNA duplex-decamer containing the (6-4)
663 photoproduct of thymidylyl(3'-->5')thymidine by NMR and relaxation matrix refinement. *Eur*
664 *J Biochem* **228**, 849-854 (1995).

665
666 54. Hwang GS, Kim JK, Choi BS. NMR structural studies of DNA decamer duplex containing the
667 Dewar photoproduct of thymidylyl(3'-- >5')thymidine. Conformational changes of the
668 oligonucleotide duplex by photoconversion of a (6-4) adduct to its Dewar valence isomer.
669 *Eur J Biochem* **235**, 359-365 (1996).

670
671 55. Svoboda DL, Smith CA, Taylor JS, Sancar A. Effect of sequence, adduct type, and opposing
672 lesions on the binding and repair of ultraviolet photodamage by DNA photolyase and (A)BC
673 excinuclease. *J Biol Chem* **268**, 10694-10700 (1993).

674
675 56. Sugasawa K, Okamoto T, Shimizu Y, Masutani C, Iwai S, Hanaoka F. A multistep damage
676 recognition mechanism for global genomic nucleotide excision repair. *Genes Dev* **15**, 507-
677 521 (2001).

678
679 57. Jiang W, Bikard D, Cox D, Zhang F, Marraffini LA. RNA-guided editing of bacterial genomes
680 using CRISPR-Cas systems. *Nat Biotechnol* **31**, 233-239 (2013).

681
682 58. Pyne ME, Moo-Young M, Chung DA, Chou CP. Coupling the CRISPR/Cas9 System with
683 Lambda Red Recombineering Enables Simplified Chromosomal Gene Replacement in
684 Escherichia coli. *Appl Environ Microbiol* **81**, 5103-5114 (2015).

685
686 59. Tokunaga M, Imamoto N, Sakata-Sogawa K. Highly inclined thin illumination enables clear
687 single-molecule imaging in cells. *Nat Methods* **5**, 159-161 (2008).

688
689 60. Schindelin J*, et al.* Fiji: an open-source platform for biological-image analysis. *Nat Methods* **9**,
690 676-682 (2012).

691
692 61. Ghodke H*, et al.* Spatial and temporal organization of RecA in the Escherichia coli DNA-
693 damage response. *Elife* **8**, (2019).

694

695

696

697 **Figure legends**

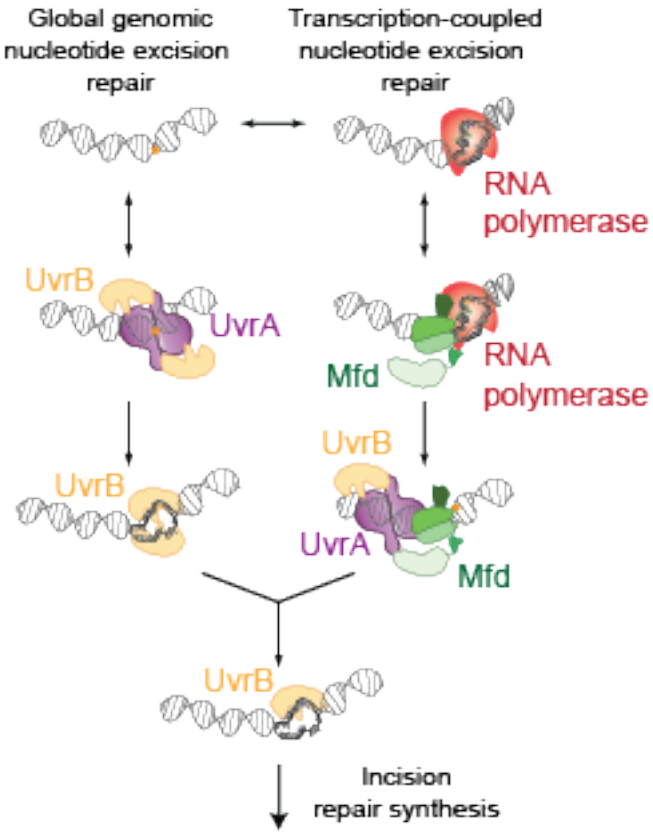

698 Figure 1

699 **Figure 1: Nucleotide excision repair in *Escherichia coli***

700 Damage detection in nucleotide excision repair in *E. coli* proceeds *via* global damage surveillance
701 executed by $UvrA_2$(B), and RNA polymerase transcribing damaged template DNA. The UvrA dimer
702 loads UvrB which verifies the presence of DNA damage in a strand-specific manner. Alternately, stalled
703 elongation complexes at the site of DNA damage are rescued by the transcription repair coupling
704 factor Mfd, which in turn recruits $UvrA_2$(B) to the site of the stalled RNAP. This is followed by strand-
705 specific loading of UvrB at the site of the lesion. Following damage verification by UvrB, a single-
706 stranded patch of DNA containing the damage is incised by the UvrC endonuclease. This is followed
707 by repair synthesis and ligation coordinated by UvrD, PolI and LigA.

708

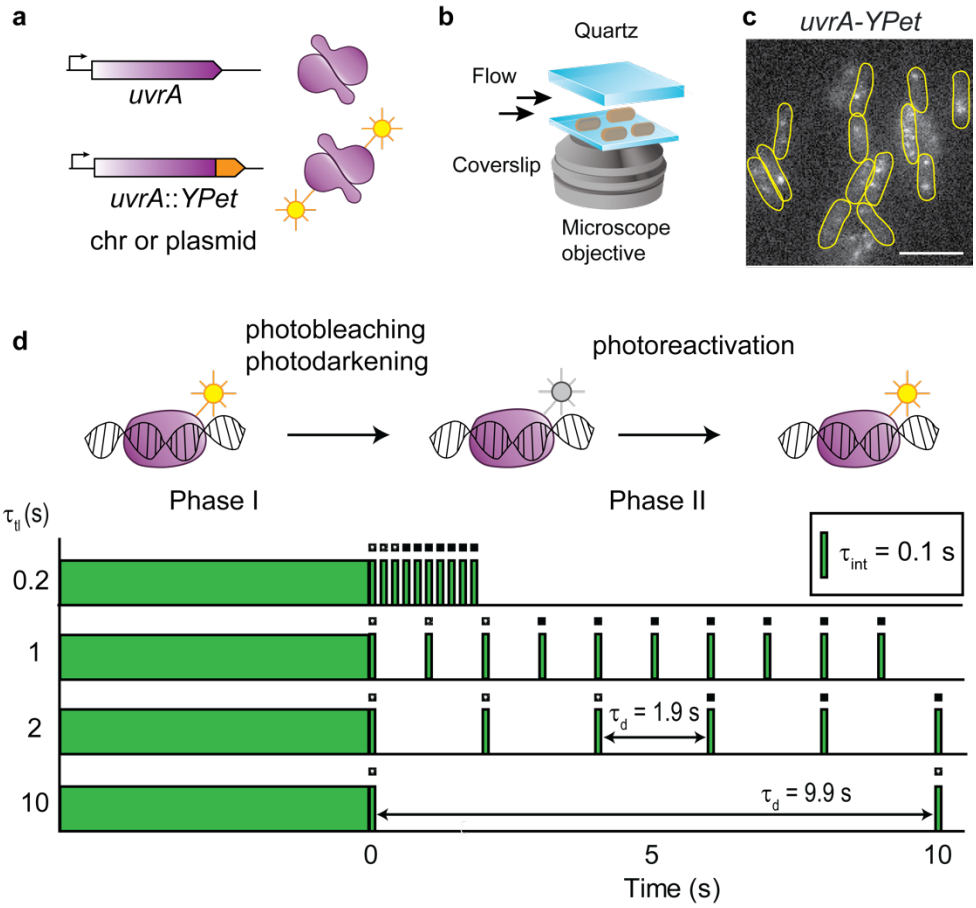

Figure 2

Figure 2: Construction of *uvrA-YPet* and imaging of UvrA-YPet

a. A chromosomal fusion of UvrA to the yellow fluorescent protein (YPet) under the native *uvrA* locus was created using λ Red recombination in MG1655 cells. In a second approach, the *uvrA-YPet* allele was expressed under the native *uvrA* promoter from a low-copy plasmid in Δ*uvrA* cells.

b. Cells expressing fluorescent UvrA-YPet were grown to early exponential phase and loaded in a flow cell. Cells were imaged under constant supply of aerated growth medium for several hours.

c. Fluorescence images of UvrA-YPet reveal a mixture of foci and diffuse cellular background signal. Scale bar represents 5 µm. Cell outlines are provided as a guide to the eye.

d. Schematic of interval imaging approach employed to measure the off rates of fluorescently tagged proteins in cells. Each acquisition is collected in two phases. In the first phase, fluorescent signal is bleached to enable observation of single fluorescent YPet molecules. In the second phase, a dark frame τ_d is introduced such that the time-lapse time $\tau_{tl} = \tau_d + \tau_{int}$, where τ_{int} is the integration time (100

722 ms). In this phase, the lifetimes of individual binding events of UvrA-YPet molecules are measured and
723 combined to obtain a cumulative residence time distribution.

724

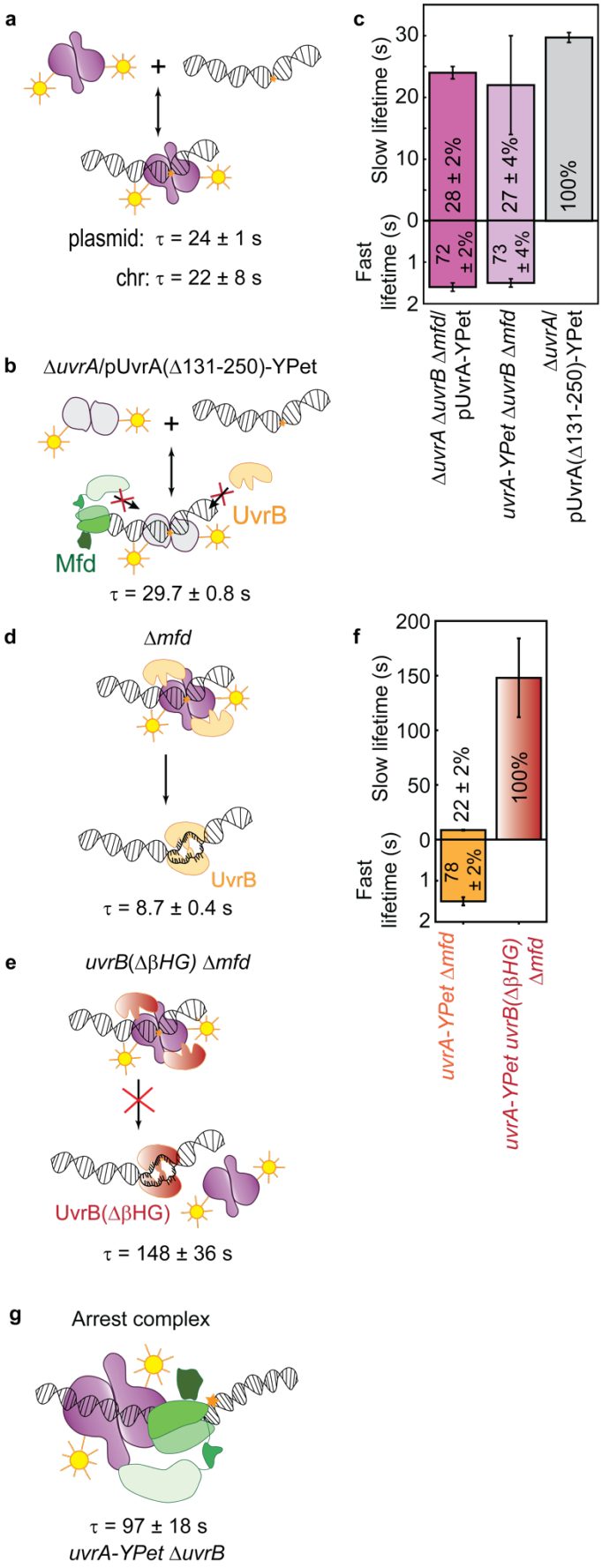
a
plasmid: τ = 24 ± 1 s
chr: τ = 22 ± 8 s
b
ΔuvrA/pUvrA(Δ131-250)-YPet
UvrB
Mfd
τ = 29.7 ± 0.8 s
c
Slow lifetime (s)
Fast lifetime (s)
28 ± 2%
72 ± 2%
27 ± 4%
73 ± 4%
100%
ΔuvrA ΔuvrB Δmfd/ pUvrA-YPet
uvrA-YPet ΔuvrB Δmfd
ΔuvrA/ pUvrA(Δ131-250)-YPet
d
Δmfd
UvrB
τ = 8.7 ± 0.4 s
e
uvrB(ΔβHG) Δmfd
UvrB(ΔβHG)
τ = 148 ± 36 s
f
Slow lifetime (s)
Fast lifetime (s)
22 ± 2%
78 ± 2%
100%
uvrA-YPet Δmfd
uvrA-YPet uvrB(ΔβHG) Δmfd
g
Arrest complex
τ = 97 ± 18 s
uvrA-YPet ΔuvrB

Figure 3

726 **Figure 3: DNA binding lifetimes of UvrA-YPet in the presence of UvrB**

727 **a.** Kinetics of UvrA-YPet interactions with DNA can be detected in the absence of UvrB and Mfd, in
728 Δ*uvrA* Δ*uvrB* Δ*mfd* cells expressing UvrA-YPet from a low-copy plasmid or in Δ*uvrB* Δ*mfd* cells
729 expressing UvrA-YPet from the chromosome.

730 **b**. Cartoon illustrates DNA binding by the mutant UvrA(Δ131-250)-YPet, which is defective in
731 interacting with UvrB and Mfd.

732 **c.** Bar plots represent lifetimes of DNA-bound UvrA-YPet (plasmid: n = 34,927 counts from 5 repeats;
733 chromosomal: n = 970r counts from 3 repeats) and mutant UvrA(Δ131-250)-YPet (a total of n = 88,232
734 counts from 4 repeats) in the corresponding genetic background. Lifetimes were obtained from
735 globally fitting the cumulative residence time distributions (CRTDs) (see also Supplementary Fig. 2a -
736 f). Where two kinetic sub-populations are detected, the fast lifetime is displayed in the lower panel.
737 Percentage represents the amplitude of kinetic sub-populations. Error bars are standard deviations
738 from ten bootstrapped CRTDs. See also source data file.

739 **d.** Cartoon illustrates loading of UvrB by UvrA. This may occur at sites of undamaged or damaged DNA.

740 **e.** Cartoon illustrates the complex formed by UvrA and the mutant UvrB(ΔβHG) that is deficient in
741 loading reaction.

742 **f.** Bar plots represent lifetimes of DNA-bound UvrA-YPet in Δ*mfd* cells expressing either wild-type UvrB
743 (n = 29,743 counts from 11 repeats) or mutant UvrB(ΔβHG) (n = 16,353 counts from 2 repeats).
744 Lifetimes were obtained from globally fitting the CRTDs, with more than 1,000 counts each CRTD (see
745 Supplementary Fig. 2g - j). Where two kinetic sub-populations are detected, the fast lifetime is
746 displayed in the lower panel. Percentage represents the amplitude of kinetic sub-populations. Error
747 bars are standard deviations from ten bootstrapped CRTDs. See also source data file.

748 **g.** Cartoon of the arrested Mfd-UvrA complex. See also Supplementary Figure 3 a-b.

749

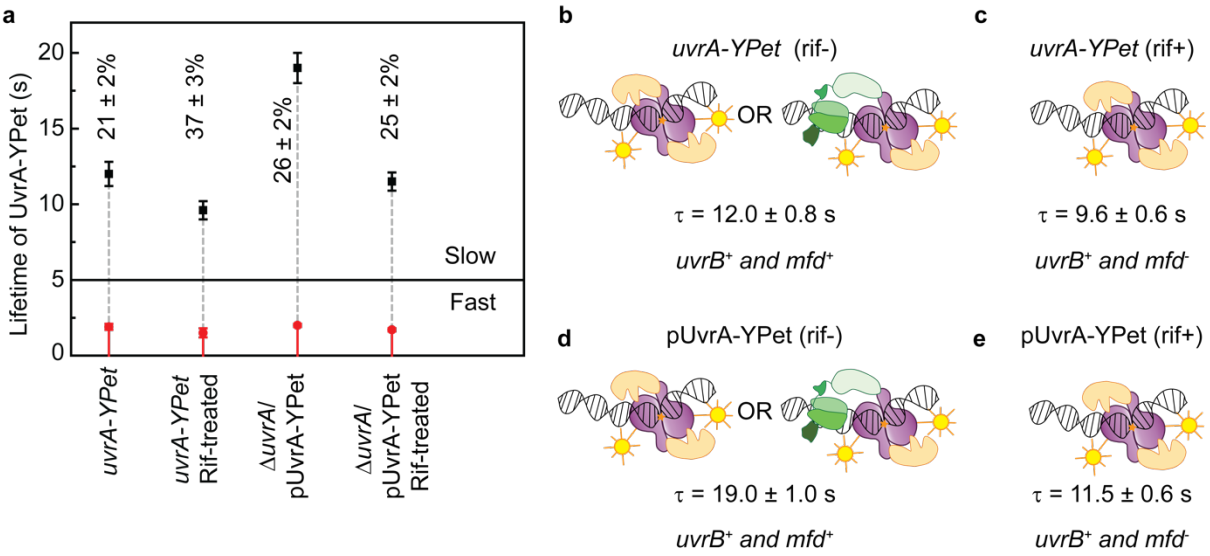

Figure 4

Figure 4: Dissociation kinetics of UvrA-YPet in TCR-competent cells

a. Lifetimes of UvrA-YPet in *uvrA-YPet* cells or Δ*uvrA*/pUvrA-YPet cells untreated or treated with rifampicin. Lifetimes were obtained from globally fitting the CRTDs (see Supplementary Figure 4 a, c, e, g). Slow lifetime is presented in black. Fast lifetime is presented in red. Percentages represent the amplitude of the slowly dissociating population. Error bars are standard deviations from ten bootstrapped CRTDs. See also source data file.

b. In the presence of UvrB and Mfd, UvrA-YPet in *uvrA-YPet* cells exhibited a slow lifetime of 12.0 ± 0.8 s, reflecting UvrA interactions with UvrB and Mfd (n = 20,111 counts from 8 repeats).

c. Rifampicin treatment abolishes Mfd-RNAP interactions, hence, UvrA-YPet is channelled towards interactions with UvrB, with the slow lifetime was found to be 9.6 ± 0.6 s (n = 15,355 counts from 3 repeats).

d. When UvrA-YPet concentration increased eight fold via the means of plasmid expression, the slow lifetime of UvrA-YPet in Δ*uvrA*/pUvrA-YPet cells was found to be 19 ± 1 s, longer than that of UvrA-YPet in *uvrA-YPet* cells (12 s) (n = 19,853 counts from 3 repeats).

e. Upon rifampicin treatment, the slow lifetime of UvrA-YPet in Δ*uvrA*/pUvrA-YPet cells reduced to 11.5 ± 0.6 s (n = 31,788 counts from 4 repeats).

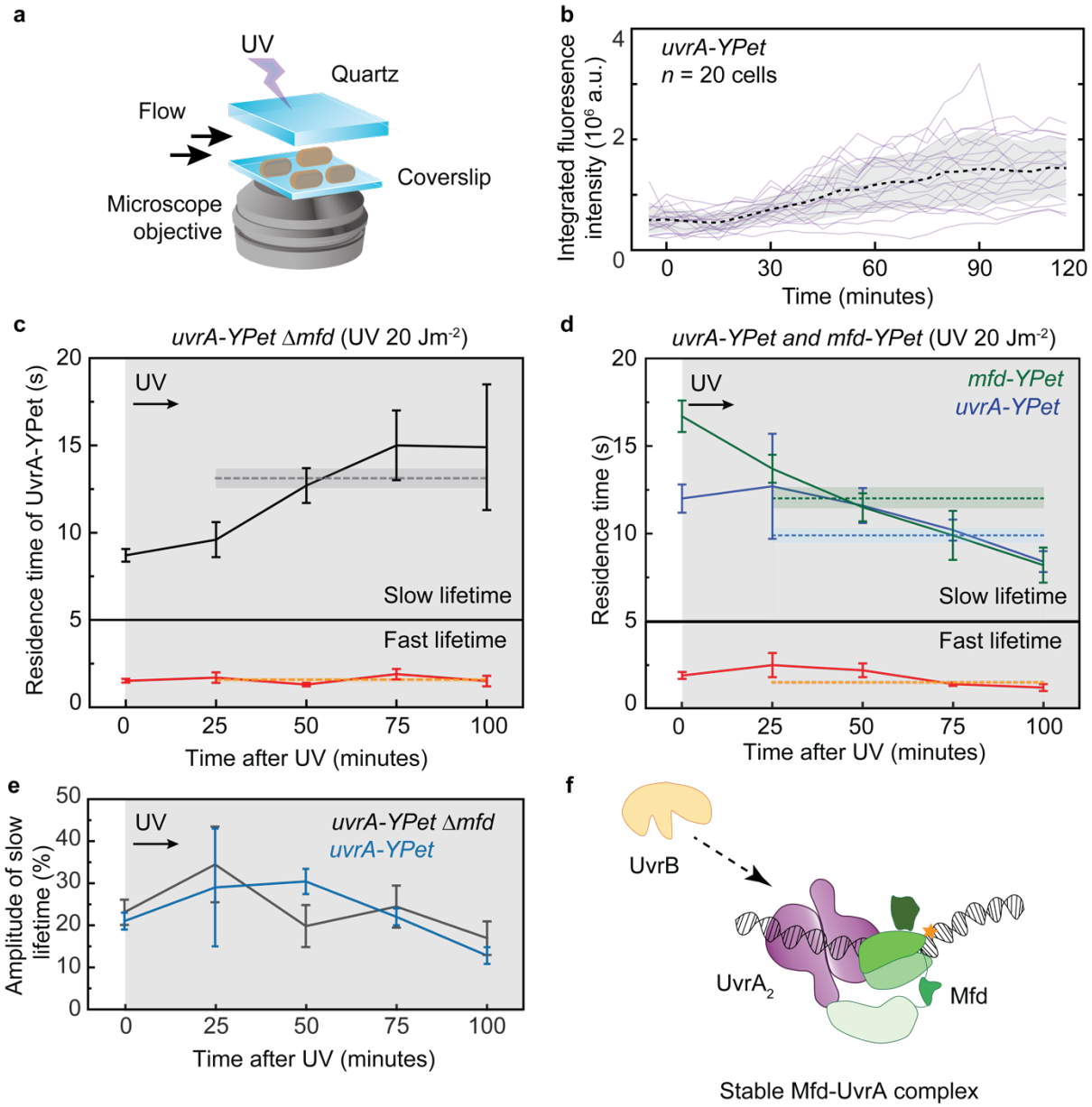

Figure 5

Figure 5: Lifetimes of DNA-bound UvrA and Mfd in response to UV irradiation

a. Experimental setup for introducing UV damage followed by interval imaging. A 20 Jm^{-2} dose of UV (254 nm) light is provided *via* a quartz window in the flow cell. This setup enables imaging of cells at 30 °C for several hours after UV.

b. Fluorescence intensity of single *uvrA-YPet* cells increases following exposure to UV light, indicating that expression of UvrA-YPet is upregulated in the SOS response.

775 **c.** Lifetimes of UvrA-YPet in TCR-deficient cells as a function of time following UV exposure. Lifetimes
776 were obtained from globally fitting the CRTDs (see Supplementary Fig. 5a-d). Error bars are standard
777 deviations from ten bootstrapped CRTDs. Lifetimes of the fast and slowly dissociating sub-populations
778 are shown in the lower and upper panels respectively. Dashed lines represent lifetimes obtained from
779 aggregated CRTDs within 100 minutes following UV exposure. The lifetimes at t = 0 minutes represent
780 those of UvrA-YPet in TCR-deficient cells during normal growth and are reproduced from Fig. 4a. (After
781 UV irradiation *uvrA-YPet* Δ*mfd* all data: n = 21,824 counts from 4 repeats; 0 – 25 min: n = 3243; 25 -50
782 min: n = 5175; 50 -75 min: n = 6079; 75 – 100 min: n = 5999 counts).

783 **d.** Lifetimes of UvrA-YPet in *uvrA-YPet* cells (blue) (After UV irradiation *uvrA-YPet* all data: n = 25,935
784 counts from 4 repeats; 0 – 25 min: n = 5359; 25 -50 min: n = 8070; 50 -75 min: n = 7481; 75 – 100 min:
785 n = 4983 counts) or Mfd-YPet in *mfd-YPet* cells (green) (After UV irradiation *mfd-YPet* all data: n =
786 14,553 counts from 4 repeats; 0 – 25 min: n = 5133; 25 -50 min: n = 3846; 50 -75 min: n = 3119; 75 –
787 100 min: n = 2286 counts) as a function of time following UV exposure. Lifetimes were obtained from
788 globally fitting the CRTDs (see Supplementary Fig. 5a-d and Supplementary Fig. 6a-d). Error bars are
789 standard deviations from ten bootstrapped CRTDs. Dash lines and error bands represent lifetimes and
790 the corresponding standard deviations obtained from aggregated CRTDs within 100 minutes following
791 UV exposure. Fitting results are available in Table 1. The lifetimes at t = 0 minutes represent those of
792 UvrA-YPet in *uvrA-YPet* cells during normal growth and are reproduced from Fig. 4a. Lifetime of Mfd-
793 YPet at t = 0 minutes is reproduced from our previous work (ref 12).

794 **e.** Amplitudes of slowly dissociating species of UvrA-YPet in *mfd*$^+$ (blue) or Δ*mfd* (black) cells carrying
795 *uvrA-YPet.* See also table 1 for fitting results and source data file.

796 **f.** UvrB (orange) controls the release of UvrA (purple) from UvrA-Mfd (green) intermediates.

797

798 **Table 1: Summary of binding lifetimes**

Strain (genotype)	Probe	Treatment	A_{fast}	τ_{fast} (s)	A_{slow}	τ_{slow}	k_b (s^{-1})	Exponential fit	Figure
Δ*uvrA* Δ*uvrB* Δ*mfd*/pUvrA-YPet	UvrA-YPet (plasmid)	-	72 ± 2	1.6 ± 0.1	28 ± 2	24 ± 1	5.5 ± 0.1	2	3
uvrA-YPet Δ*uvrB* Δ*mfd*	UvrA-YPet (chr)	-	73 ± 4	1.4 ± 0.4	27 ± 4	22 ± 8	5.5 ± 0.5	2	3
Influence of Mfd and UvrB on the lifetime of UvrA in undamaged cells									
Δ*uvrA*/ pUvrA(Δ131-250)-YPet	UvrA-YPet (plasmid)	-			100	29.7 ± 0.8	5.2 ± 0.05	1	3
uvrA-YPet Δ*mfd*	UvrA-YPet (chr)	-	78 ± 2	1.5 ± 0.1	22 ± 2	8.7 ± 0.4	6.3 ± 0.2	2	3
uvrA-YPet uvrB(Δ*βHG*) Δ*mfd*	UvrA-YPet (chr)	-			100	148 ± 36	6.0 ± 0.2	1	3
uvrA-YPet Δ*uvrB*	UvrA-YPet (chr)	-	-	-	100	97 ± 18	0.010 ± 0.002	1	3
Lifetime of UvrA-YPet in untreated and rif treated cells									
uvrA-YPet	UvrA-YPet (chr)	-	79 ± 0.2	1.9 ± 0.2	21 ± 2	12.0 ± 0.8	7.2 ± 0.2	2	4
uvrA-YPet	UvrA-YPet (chr)	rif	63 ± 3	1.5 ± 0.3	37 ± 3	9.6 ± 0.6	5.7 ± 0.2	2	4
Δ*uvrA*/pUvrA-YPet	UvrA-YPet (plasmid)	-	74 ± 2	2.0 ± 0.1	26 ± 2	19 ± 1	6.8 ± 0.1	2	4
Δ*uvrA*/pUvrA-YPet	UvrA-YPet (plasmid)	rif	75 ± 2	1.7 ± 0.1	25 ± 2	11.5 ± 0.6	7.3 ± 0.1	2	4
Lifetime of UvrA-YPet in *mfd*$^-$ cells after UV damage									
uvrA-YPet Δ*mfd*	UvrA-YPet (chr)	20Jm^{-2} UVC (temporally averaged)	77 ± 3	1.6 ± 0.1	23 ± 2	13.1 ± 0.6	6.2 ± 0.2	2	5
uvrA-YPet Δ*mfd*	UvrA-YPet (chr)	20Jm^{-2} UVC (0 – 25 min)	66 ± 1	1.6 ± 0.3	34 ± 1	9.6 ± 1	5.2 ± 0.3	2	5
uvrA-YPet Δ*mfd*	UvrA-YPet (chr)	20Jm^{-2} UVC (25 – 50 min)	80 ± 5	1.3 ± 0.1	20 ± 5	13 ± 1	5.6 ± 0.4	2	5
uvrA-YPet Δ*mfd*	UvrA-YPet (chr)	20Jm^{-2} UVC (50 – 75 min)	76 ± 5	1.9 ± 0.3	24 ± 5	15 ± 2	6.7 ± 0.3	2	5
uvrA-YPet Δ*mfd*	UvrA-YPet (chr)	20Jm^{-2} UVC (75 – 100 min)	83 ± 3	1.5 ± 0.3	17 ± 3	15 ± 4	6.5 ± 0.5	2	5
Lifetime of UvrA-YPet in *mfd*$^+$ *uvrB*$^+$ cells after UV damage									

uvrA-YPet	UvrA-YPet (chr)	20Jm^{-2} UVC (temporally averaged)	74 ± 2	1.5 ± 0.1	26 ± 2	9.9 ± 0.4	5.5 ± 0.1	2	5
uvrA-YPet	UvrA-YPet (chr)	20Jm^{-2} UVC (0 – 25 min)	71 ± 0.1	2.6 ± 0.7	29 ± 0.1	12 ± 3	4.8 ± 0.1	2	5
uvrA-YPet	UvrA-YPet (chr)	20Jm^{-2} UVC (25 – 50 min)	70 ± 3	2.2 ± 0.4	30 ± 3	11.6 ± 0.9	5.9 ± 0.3	2	5
uvrA-YPet	UvrA-YPet (chr)	20Jm^{-2} UVC (50 – 75 min)	78 ± 2	1.4 ± 0.1	22 ± 2	10.2 ± 0.6	5.6 ± 0.2	2	5
uvrA-YPet	UvrA-YPet (chr)	20Jm^{-2} UVC (75 – 100 min)	87 ± 2	1.2 ± 0.2	13 ± 2	8.4 ± 0.6	5.8 ± 0.4	2	5
Lifetime of Mfd-YPet after UV damage									
mfd-YPet	Mfd-YPet (chr)	20Jm^{-2} UVC (temporally averaged)			100	12.0 ± 0.6	6.0 ± 0.1	1	5
mfd-YPet	Mfd-YPet (chr)	20Jm^{-2} UVC (0 – 25 min)			100	13.7 ± 0.8	5.2 ± 0.2	1	5
mfd-YPet	Mfd-YPet (chr)	20Jm^{-2} UVC (25 – 50 min)			100	11.5 ± 0.8	6.0 ± 0.2	1	5
mfd-YPet	Mfd-YPet (chr)	20Jm^{-2} UVC (50 – 75 min)			100	10 ± 1	6.9 ± 0.2	1	5
mfd-YPet	Mfd-YPet (chr)	20Jm^{-2} UVC (75 – 100 min)			100	8 ± 1	6.4 ± 0.3	1	5